INNOVATIVE SUBSTRUCTURE DESIGN AND MODELING OF THE JEWFISH CREEK BRIDGE PROJECT

John S. Hartland, PE, Jacobs Engineering Group, Tampa, FL

ABSTRACT

In October 2004 the design build team of Granite/Jacobs was awarded the contract to replace an existing bascule bridge over Jewfish Creek in Key Largo, Florida with a 7410' long bridge. The new bridge consists primarily of simply-supported prestressed concrete beams, supported on drilled shaft bents. The design wind loading for the bridge, which governed the substructure design, is 120% of the design wind pressure required by the AASHTO LRFD Specifications. Using the conventional design approach of modeling the bent as a cantilevered beam, free to rotate in the longitudinal direction, would result in millions of dollars in increased construction costs.

By developing a three dimensional model of the bridge, the longitudinal rotational stiffness at each pier was determined. Incorporating this stiffness in the design of the substructure reduced the design forces in the substructure and allowed the reduction of up to 50% of the reinforcement in the drilled shafts and columns. The results of the analysis indicated that for a typical simply supported prestressed beam bridge with a continuous deck, the longitudinal rotational stiffness of the superstructure can be defined as a function of the rotational stiffness of the two rows of bearings at each pier. Depending on the continuity of the pier under investigation, as well as the continuity of the adjacent piers, the superstructures rotational stiffness ranges from 55% to 95% of the bearings rotation stiffness. This paper provides a detail description of the design and modeling procedure, as well as providing guidelines for the estimating the superstructure rotational stiffness to be used in the design of the substructure.

Keywords: Flexibility, Stiffness, Prestressed, Beam, Substructure, Superstructure, Bridge, Elastic, Foundation, Wind, Design, Model, Bearing, Deflection, Rotation, Cantilever, LRFD, Innovative

INTRODUCTION

In October 2004, the design-build team of Granite/Jacobs was awarded the contract to replace an existing bridge carrying US-1 over Jewfish Creek in Key Largo, Florida. The existing bridge, built in the mid 1940's, is a 225' long, two lane, low level, double leaf bascule structure. A 5,000 foot long causeway dividing Lake Surprise provides the South approach to the bridge as well as providing access to businesses located on the south side of Jewfish Creek (see Figures 1 & 2). The project incorporates the removal of the existing bridge and 4,000 feet of the causeway and replacing it with a 7,410 foot long bridge.

Figure 1 – Project Layout

Figure 2 – Existing Bridge and Causeway

The majority of the superstructure consists of simply supported FBT-78 and modified FBT-72 prestressed beams with a continuous cast-in-place deck between expansion joints and span lengths ranging from 90'-2" to 160'-0'. Over Jewfish Creek, a three-span continuous unit (150'-160'-150') is constructed to provide the redundancy in the superstructure to transfer ship impact forces to adjacent piers. The continuity is developed through mild reinforcement extending beyond the ends of the beam into the diaphragm in the positive moment region as well as additional reinforcement in the deck for the negative moment region. Due to the necessity for entrance and exit ramps on the south and north sides of Jewfish Creek, the cross section varies to accommodate the acceleration and deceleration lanes. Figure 3 provides the typical 58'-1" wide cross-section of the bridge, which provides one lane in each direction with 6'-0" inside shoulders, a 7'-0" outside southbound shoulder and a 10'-0" outside northbound shoulder. The wider shoulder in the northbound direction allows for an additional traffic lane during emergency hurricane evacuation of the Keys. At the entrance and exit ramps, the deck width increases to a maximum of 122'-3" to accommodate the additional lane in each direction, as well as a gore area between the lanes (see Figure 4).

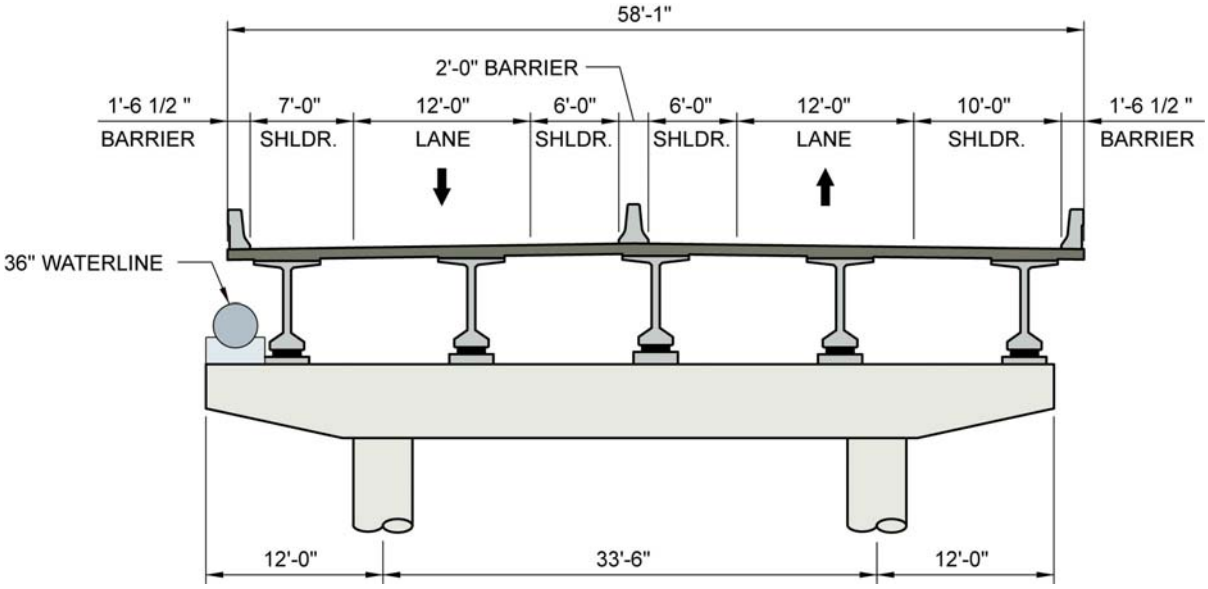

Figure 3 – Typical Section

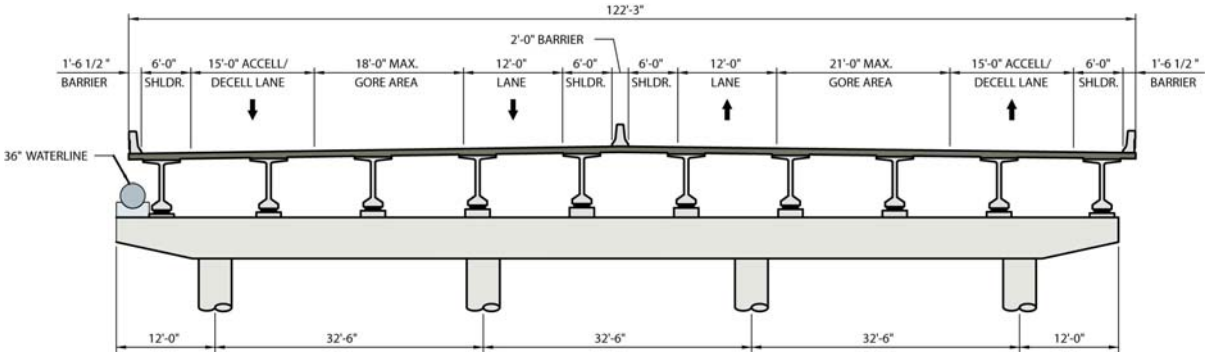

Figure 4 – Section at Access Ramps

The vertical profile of the bridge consist of a crest curve over Jewfish Creek with grades of approximately (+)3.00% and (-)3.00%. The profile provides the minimum vertical clearance of 65'-0" over the Jewfish Creek channel. For the low level portion of the bridge which replaces the causeway through Lake Surprise, a (+)0.30% grade is provided for drainage. The minimum vertical clearance for this section of the project is 14'-0".

The typical substructure unit is a cast in place bent cap on two, three or four drilled shafts, depending on the superstructure width (see Figures 3 and 4). Two different shaft diameters were incorporated into the design - 48" and 60". For the two piers on either side of the channel that are susceptible to ship impact, the substructure consist of six, 48" diameter drilled shafts with a waterline footing, three 60" diameter columns and a pier cap. The general subsurface soil conditions consist of a 10'-0" deposit of organic peat above the Key Largo Limestone Formation.

DESIGN WIND LOAD

During the proposal phase of the project, there was some ambiguity regarding the magnitude of the design wind loading for the bridge. When a project is being designed according to the AASHTO Standard Specifications, the Florida Department of Transportation's Structures Design Guidelines (SDG) provides the values of the design wind pressures based on the height of the structure. For the South Florida area, it was also required to add 20% to these pressures due to the higher wind speeds encountered in the area. For designs governed by the AASHTO LRFD Specification, the SDG again addresses the 20% increase in South Florida but no longer provides the wind pressures. Therefore, the wind pressures need to be calculated as per the LRFD Specification.

According to the LRFD Specification, the design wind pressure shall be determined by the following equation:

$$P_D = P_B \left(\frac{V_{DZ}}{V_B} \right)^2$$

where:

P_D = design wind pressure
P_B = base wind pressure of 50 psf as per AASHTO Table 3.8.1.2.1-1
V_B = base wind velocity of 100 mph at 30 ft above ground/water
V_{DZ} = design wind velocity (mph) at the design elevation, Z (ft), determined by following formula:

$$V_{DZ} = 2.5\, V_O \left(\frac{V_{30}}{V_B} \right) \ln\left(\frac{Z}{Z_O} \right)$$

where:

V_{30} = design wind velocity (mph) at 30 ft above low ground or design water level
Z = height of structure at which wind loads are being calculated as measured from low ground or design water level

Z_0 = friction length (ft) of upstream fetch, a meteorological wind characteristic taken as specified in AASHTO Table 3.8.1.1-1 for various upwind surface characteristics.

V_0 = friction velocity (mph), a meteorological wind characteristic taken as specified in AASHTO Table 3.8.1.1-1 for various upwind surface characteristics.

The upwind surface characteristic for this bridge location can be categorized as 'open country', which is the most severe condition. For this surface condition, the values for V_0 and Z_0 are 8.2 mph and 0.23 ft respectively.

As per the LRFD Specification, the design wind velocity at 30ft above ground/water can be established from the following:

- Fastest-mile-of-wind charts available in ASCE 7-88 for various recurrence levels
- Site-specific wind surveys
- In absence of better criterion, the assumption that $V_{30} = V_0 = 100$ mph

.

Based on the information available, it was determined that the most accurate approach was to use the wind chart from ASCE 7-88. As the chart indicates, the vast majority of the State of Florida can be categorized with a V_{30} equal to 100 mph, except for South Florida, which has a value of 110 mph. Figure 5 provides the design wind pressure for both the 100mph and 110 mph wind speed as well as the wind pressures from the SDG.

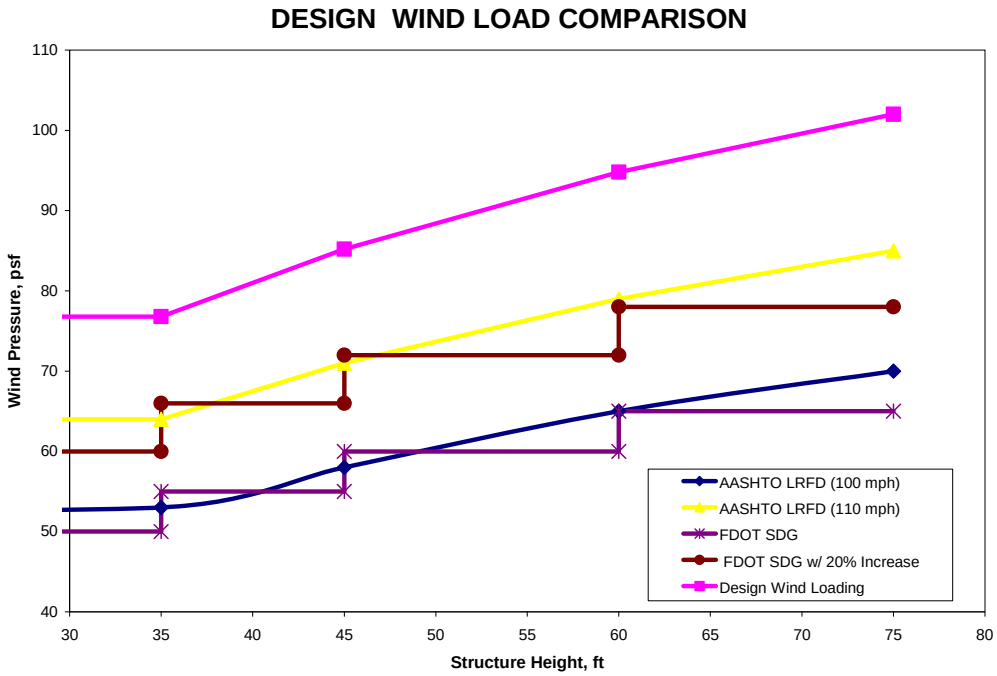

Figure 5 – Design Wind Pressure

As the graph indicates, the design wind pressures provided by the SDG for the Standard Specification correlate well with the 100mph design velocity. The 20% increase in pressure correlates with the LRFD pressures using a 110mph wind velocity. As a result, it was the design team's interpretation that the 20% increase required by the SDG applied when 100mph was used for the design wind velocity and that by using a wind velocity of 110mph, the 20% increase was already incorporated. Therefore, the preliminary design associated with the team's bid utilized a design wind velocity of 110mph without any additional increase. Unfortunately, after the project was awarded the design team was notified that the intent of the SDG was to provide a 20% increase in the pressure associated with the 110mph wind velocity. For the tall, substructure units, the longitudinal wind load governed the design of the columns and drilled shafts. Increasing the design loading by 20% would have significant cost implications to the team. As a result, a more refined approach to the substructure design was required to counteract the increased design load.

SUBSTRUCTURE DESIGN PROCEDURE

Due to the lack of full continuity of the prestressed beams, the typical practice to design the substructure is to assume that the bent is completely free at the top. Under longitudinal loads, the bent would react like a 'flag pole' with a point of fixity somewhere below the ground line, as shown in Figure 6a. However, since there are two rows of bearings at each pier associated with the simply supported prestressed beams, a rotational stiffness is provided by the superstructure due to the coupling effect of the bearings. This stiffness reduces the longitudinal rotation of the substructure and thus the bending moment in the columns and shafts, as shown in Figure 6b.

To determine the reduction of the rotation superstructure stiffness due to the lack of full continuity of the beams a stiffness analysis was performed using GTSTRUDL. The entire bridge was modeled and the rotational stiffness of the superstructure was determined at each pier. In addition, unit longitudinal and transverse uniform loads were applied over the bridge length to determine the load distribution for each pier. Due to the vast variability in the substructure and superstructure dimensions, modeling techniques were utilized to greatly simplify the model. These techniques will be discussed in more detail in subsequent sections of the paper.

Once the load distribution and the superstructure stiffness were determined, FBPIER was used to model the substructure and determine the forces in the components. The superstructure stiffness was modeled as rotational springs located at each bearing, as shown in Figure 6c.

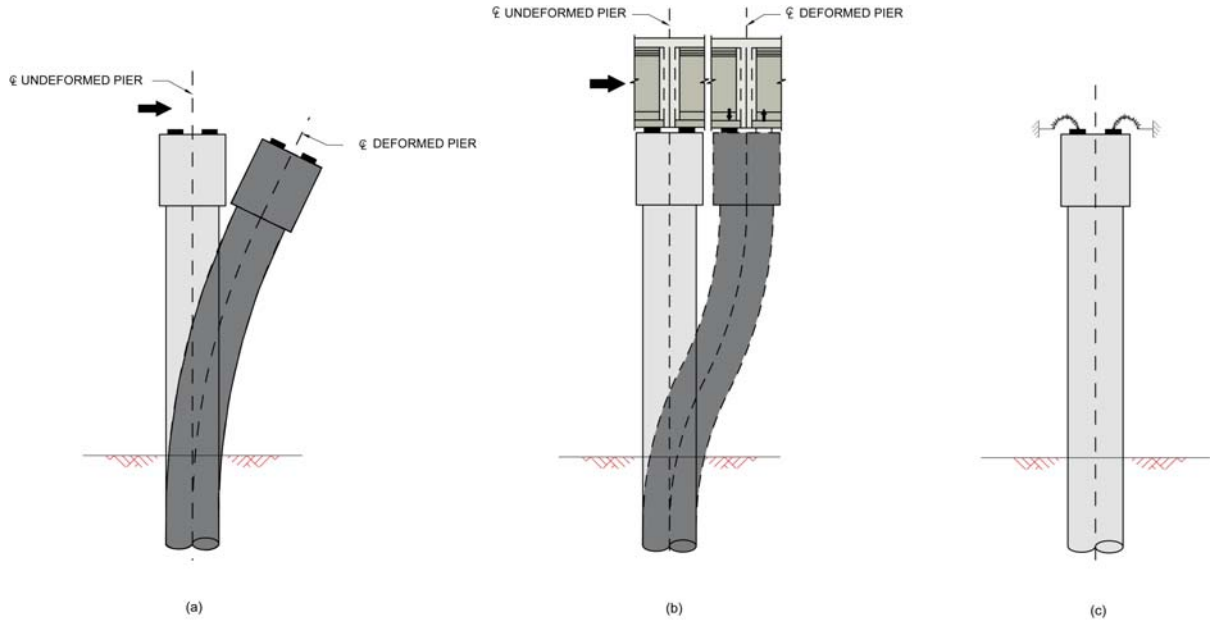

Figure 6 – (a) pier free to rotate at bearing level, (b) pier fixed for rotation due to superstructure stiffness, (c) model representing superstructure rotational stiffness

One of the key issues in the design process was the potential for uplift on the bearings. With the combination of large longitudinal forces; tall, flexible piers; and stiff bearings, the resulting vertical forces from the coupling effect of the bearings could easily exceed the dead load reaction on the bearings, especially when a load factor of 0.9 is applied to the dead load. However, this only occurred under the ultimate condition, not the service condition. It was the design team's professional opinion that uplift in the bearings was not an issue under ultimate load combinations, as long as one row of bearings could continue to resist the longitudinal and transverse forces. There may be a tendency for the bearings under uplift to be displaced, however this could be easily repaired without any significant damage occurring to the superstructure. To model the uplift condition, the bearing would need to be modeled as a nonlinear spring that represents the bilinear stiffness shown in Figure 7. Unfortunately, the client disagreed with this opinion and required that uplift not occur under any load combination. To accomplish this, the stiffness of the bearings was reduced by increasing the thickness and reducing the plan dimensions. Although this reduced the serviceability of the bearings, the dimensions were able to be changed to meet the uplift criteria while also meeting the LRFD design criteria of the bearings. A more detailed description of the bearing stiffness follows.

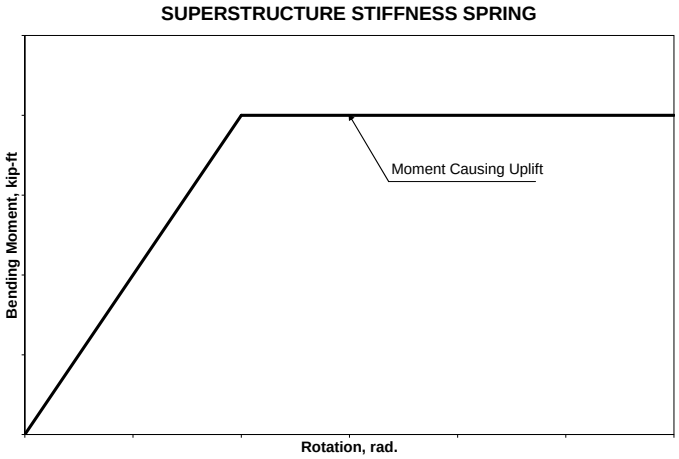

Figure 7 – Bilinear Rotational Stiffness

GTSTRUDL MODEL OF BRIDGE

Figure 8 provides the diaphragm details at interior and expansion piers typically used in Florida for prestressed beam bridges. For the interior pier location, a 9” diaphragm is constructed on either side of the pier centerline. Thin masonite boards are typically placed between the two diaphragms to act as a bond breaker, but the 8” slab is continuous over the pier. The prestressed beams are embedded approximately 4” into the diaphragm. The detail of the diaphragm at the expansion pier is similar, except a 1” gap is provided between the two diaphragms and the slab is not continuous.

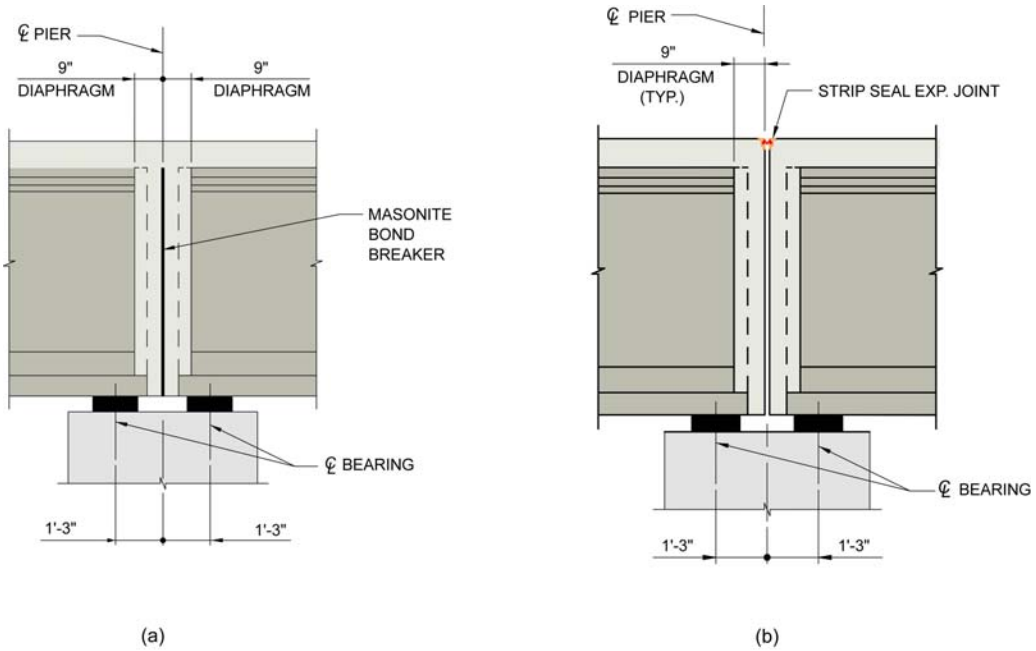

Figure 8 – (a) interior pier diaphragm, (b) expansion joint diaphragm

Figure 9 provides the schematic of how these two conditions were modeled in GTSTRUDL. The beams and slab are modeled as a beam element located along the center of gravity of the superstructure. At the bearing locations, a vertical member is defined from the CG of the superstructure to the top of the bent cap. The member property of this element is defined using a 6x6 flexibility matrix representing the properties of the bearings. In GTSTRUDL, when the flexibility matrix is used to define the member properties, the coefficients are applied to the end of the member while the beginning of the member is fixed from displacing. By properly orienting the local axis of the vertical member, the stiffness of the bearings can be modeled accurately. Horizontal rigid members are used to connect the bearing member to the vertical member representing the substructure. Similar to the bearing member, the properties of the member representing the substructure is defined using the 6x6 flexibility matrix. Since the matrix includes the effects of material properties, member properties and the actual length of the member, the modeled length of the member is irrelevant. The member is fixed at the bottom (i-node), so the flexibility is applied to the top of the bent.

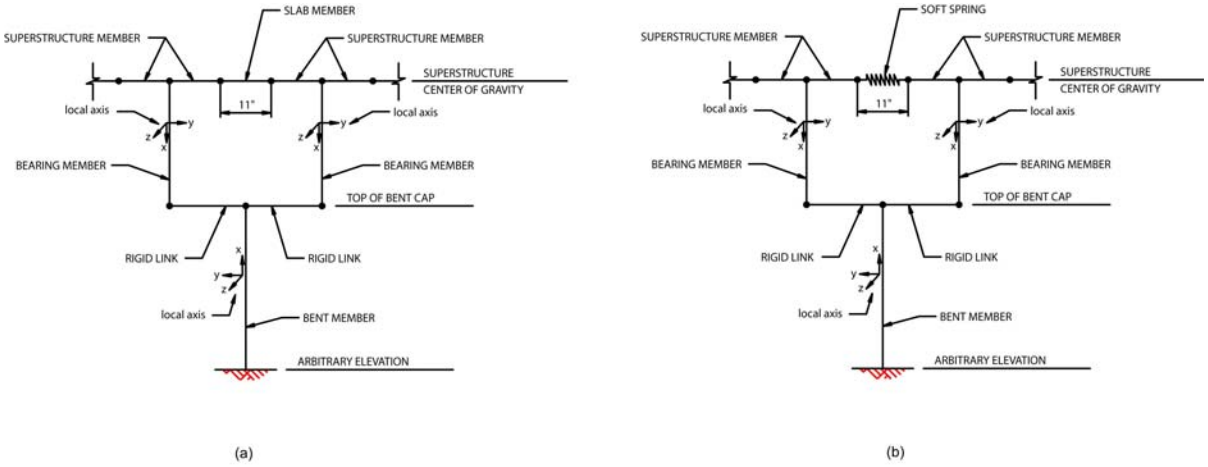

Figure 9 – Model of Pier in GTSTRUDL (a) Interior Pier, (b) Expansion Joint Pier

The modeling of the continuous slab and diaphragms was given considerable thought since it was believed that this detail would have a significant impact on the rotational stiffness of the superstructure. Due to the tendency for the deck to crack along the centerline of the pier due to the drastic reduction in stiffness, it was decided to consider the slab member between the beams to be hinged at this location. The longitudinal force applied to the superstructure would result in coupling forces between the bearings, so the slab would have to be able to transfer the shear force. Since the slab was modeled as a hinged member, there was no need to model the slab member at the center of gravity of the slab. Instead, it was modeled along the centerline of the superstructure. For the expansion joint piers, the slab member was replaced with a very soft longitudinal spring that offered no stiffness to the structure. The purpose of this spring was to easily determine the differential displacement between the adjacent units, which would be used for the design of the expansion joint movements.

To determine the superstructure's rotational stiffness at any pier, the 6x6 flexibility matrix for the pier under investigation was modified to make the substructure stiffness negligible. A bending moment was then applied at the centerline of the pier to the rigid links between the bearings. The rotational stiffness of the superstructure was then calculated by dividing the magnitude of the bending moment by the rotation of the rigid member between the bearings.

SUBSTRUCTURE FLEXIBILITY

The flexibility of a typical bent is influenced by three main elements – the soil stiffness, columns/shafts and the neoprene bearings. Each one has its individual flexibility characteristics which are combined to form the overall flexibility of the substructure. The substructure deformation resulting from horizontal force, *F*, and bending moment, *M*, (see Figure 10), can be defined by the following:

$$\Delta = F_{12_p} M + \left(F_{11_p} + F_{11_n}\right)F$$

$$\phi = \left(F_{22_p} + F_{22_n}\right)M + F_{12_p} F$$

where F_{11_p} and F_{11_n} are the translational flexibility coefficients of the pier and the neoprene bearings, respectively, due to the application of a unit shear force. F_{22_p} and F_{22_n} are the rotational flexibility coefficients of the pier and the neoprene bearings, respectively, due to the application of a unit moment. F_{12_p} is the translation/rotation (cross flexibility) coefficient of the pier. The cross flexibility coefficient for the neoprene bearings, F_{12_n}, is zero because there is no rotation in the bearings under the effect of horizontal loads or horizontal displacement under the effect of a bending moment.

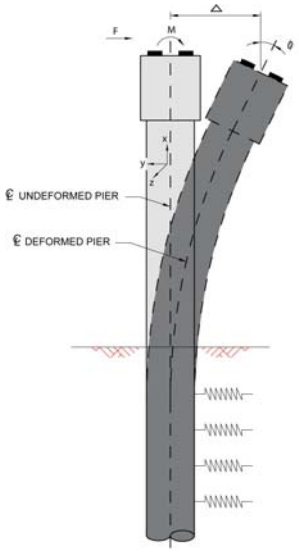

Figure 10 – Longitudinal Pier Deflection

This can be expanded to all six degrees of freedom to provide the necessary flexibility coefficients that need to be defined in order to accurately model the substructure properties. The typical member flexibility equation for the local axis member provided in Figure 10 can be written in the following form:

$$\begin{bmatrix} \Delta_x \\ \Delta_y \\ \Delta_z \\ \Theta_x \\ \Theta_y \\ \Theta_z \end{bmatrix} = \begin{bmatrix} F_{tx} & 0 & 0 & 0 & 0 & 0 \\ 0 & F_{ty} & 0 & 0 & 0 & F_{ty\_rz} \\ 0 & 0 & F_{tz} & 0 & -F_{tz\_ry} & 0 \\ 0 & 0 & 0 & F_{rx} & 0 & 0 \\ 0 & 0 & -F_{ry\_tz} & 0 & F_{ry} & 0 \\ 0 & F_{rz\_ty} & 0 & 0 & 0 & F_{rz} \end{bmatrix} \cdot \begin{bmatrix} F_x \\ F_y \\ F_z \\ M_x \\ M_y \\ M_z \end{bmatrix}$$

Take note of the sign of the off diagonal terms in the flexibility matrix. The sign of these terms depend on the local axis system of the member. Based on the local axis shown in Figure 10, a positive deflection in the *z* direction would produce a negative rotation about the *y* axis. Similarly, a positive rotation about the local y axis would produce a negative horizontal about the z axis. Therefore, these terms are negative. It should also be noted that the terms F_{ry_tz} and F_{tz_ry} are equal, as are F_{rz_ty} and F_{ty_rz}.

BEARING FLEXIBILITY

As previously discussed, the cross terms for the bearing flexibility matrix are equal to zero. Therefore, the flexibility matrix for the bearing members with the local axis shown in Figure 9 is given by the following form:

$$[F] = \begin{bmatrix} F_{tx} & 0 & 0 & 0 & 0 & 0 \\ 0 & F_{ty} & 0 & 0 & 0 & 0 \\ 0 & 0 & F_{tz} & 0 & 0 & 0 \\ 0 & 0 & 0 & F_{rx} & 0 & 0 \\ 0 & 0 & 0 & 0 & F_{ry} & 0 \\ 0 & 0 & 0 & 0 & 0 & F_{rz} \end{bmatrix}$$

For a single neoprene bearing, the axial, rotation and shear deformation can be defined by the following[1]:

$$\Delta_c = \frac{h_{rt}}{3G\left(1 + 2kS^2\right)A} N$$

$$\Theta = \frac{h_{rt}}{3G\left(1+2kS^2\right)I}M$$

$$\Delta_v = \frac{h_{rt}}{GA}V$$

where Δ_c is the compressive deflection of the bearing resulting from axial load, N; Θ is the rotational deformation of the bearing resulting from bending moment, M; Δ_v is the horizontal deflection resulting from lateral load, V; h_{rt} is the total thickness of all elastomer layers, G is the shear modulus of the elastomer (14.4 ksi), S is the shape factor, A is the plan area of the bearing, I is the moment of inertia of the bearing and k is a coefficient dependent upon neoprene hardness (0.75 for 50 durometer hardness).

Therefore, for n number of bearings in one row, the flexibility coefficients F_{tx}, F_{ty}, F_{tz} and F_{rz} are defined as follows:

$$F_{tx} = \frac{h_{rt}n}{3G\left(1+2kS^2\right)A}$$

$$F_{.ty} = F_{tz} = \frac{h_{rt}n}{GA}$$

$$F_{rz} = \frac{h_{rt}n}{3G\left(1+2kS^2\right)I}$$

The rotational flexibility of a row of bearings about the longitudinal local axis, y, is related to rotational flexibility of each bearing about is own centerline as well as the vertical flexibility of the bearing and its distance away from the centerline of the pier, d. This can be expressed by the following:

$$F_{ry} = \sum_{i=1}^{n}\left[\frac{h_{rt\,i}}{3G_i\left(1+2k_iS_i^2\right)I_i} + \frac{h_{rt\,i}}{3G_i\left(1+2k_iS_i^2\right)A_id_i^2}\right]$$

The second term, which is the term relating to the vertical flexibility and the distance from the centerline of the pier, has the most influence on the overall flexibility of the row of bearings. In fact, the first term could be disregarded without any significant loss of accuracy. However, if the first term is included, the reciprocal of each term should be added together with the reciprocal of the summation equal to the flexibility coefficient.

Similarly, the rotational flexibility about the vertical local axis, x, is related to the translational flexibility of the bearings and the distance of the bearing from the centerline of the pier. This is expressed by the following:

$$F_{rx} = \sum_{i=1}^{n} \frac{h_{rt\,i}}{G_i A_i} d_i^2$$

SUBSTRUCTURE FLEXIBILITY

To incorporate the effects of the shaft-soil interaction, the bent flexibility coefficients are based on the theory of a semi-infinite beam on an elastic foundation[2]. This theory applies for piles with length, ℓ, that meets the following criteria:

$$\ell > \frac{\pi}{\lambda} \qquad \text{where}$$

$$\lambda = \sqrt[4]{\frac{k_s d}{4EI}}$$

where k_s is the lateral subgrade modulus of the soil, d is the pile diameter or width, I is the pile moment of inertia and E is the pile concrete modulus of elasticity.

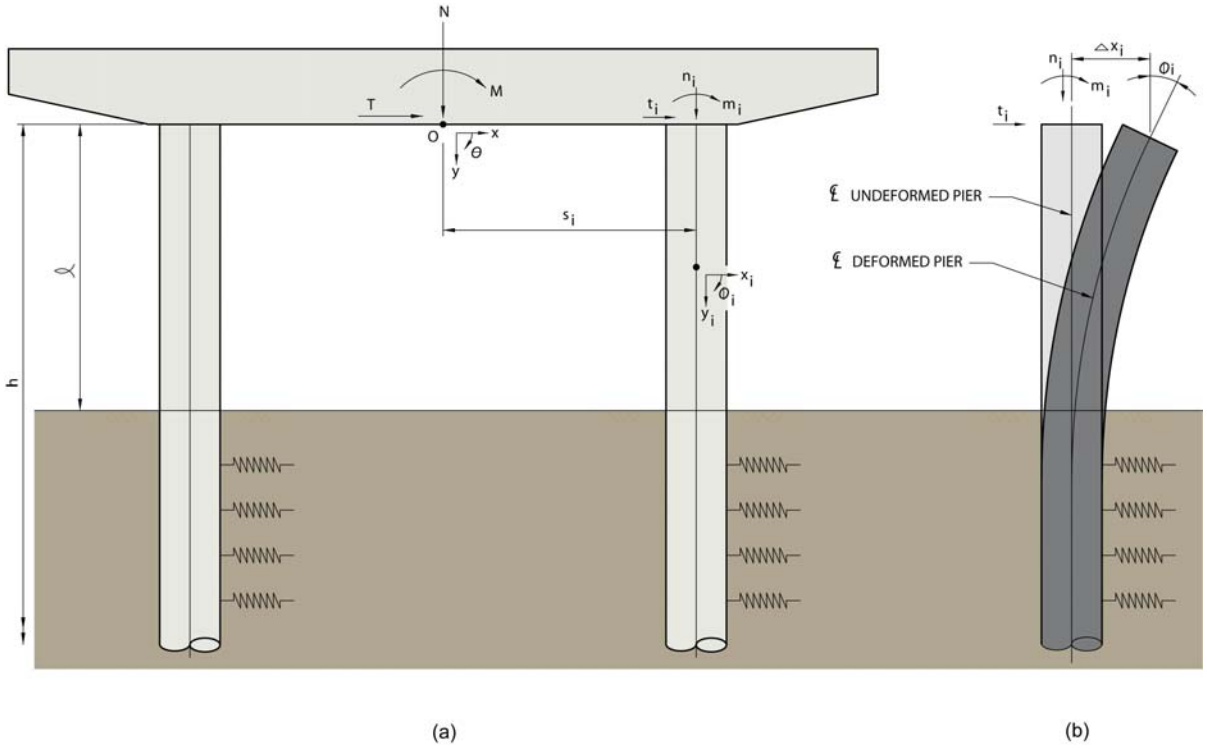

Figure 11 – Bent Deflection in Transverse Direction

If we consider the displacement of the bent in the transverse direction as shown in Figure 11a, we can define equations of equilibrium, deformation and compatibility for the bent

under applied loads *M*, *T* and *N* at point *O*. Using these equations, we can solve for the flexibility coefficients of the bents. The following are the three equations of equilibrium:

$$\sum M = 0 \quad \Rightarrow \quad M = \sum m_i + \sum n_i s_i$$

$$\sum F_x = 0 \quad \Rightarrow \quad T = \sum t_i$$

$$\sum F_y = 0 \quad \Rightarrow \quad N = \sum n_i$$

For the purpose of developing the flexibility coefficients, the individual shafts are treated as cantilever beams for the length of the beam above ground and as a semi-infinite beam on an elastic foundation for the section below ground. Based on the theory developed by Hetenyi[2], the equations of deformation at the top of the shaft (see Figure 11b) can be written as follows:

$$\phi_i = \left[\frac{4\lambda_i^{\,3}}{k_s d_i} + \frac{\ell_i}{E_i I_i}\right] m_i + \left[\frac{2\lambda_i^{\,2}}{k_s d_i}\left(1 + 2\lambda_i \ell_i\right) + \frac{\ell_i^{\,2}}{2E_i I_i}\right] t_i$$

$$\Delta x_i = \left[\frac{2\lambda_i^{\,2}}{k_s d_i}\left(1 + 2\lambda_i \ell_i\right) + \frac{\ell_i^{\,2}}{2E_i I_i}\right] m_i + \left[\frac{2\lambda_i}{k_s d_i}\left(1 + 2\lambda_i \ell_i + 2\lambda_i^{\,2} \ell_i^{\,2}\right) + \frac{\ell_i^{\,3}}{3E_i I_i}\right] t_i$$

$$\Delta y_i = \frac{h_i}{E_i A_i} n_i$$

The following compatibility equations are based on the assumption that the bent cap is a rigid element (refer to Figure 11 for variable definitions):

$$\phi_i = \Theta$$

$\Delta x_i = \Delta X$ where ΔX is transverse displacement of point *O*

$\Delta y_i = \Delta Y + s_i \Theta$ where ΔY is vertical displacement of point *O*

Although it is beyond the scope of this paper, the above equations can be combined and rewritten in the following matrix form:

$$\begin{bmatrix} T \\ M \\ N \end{bmatrix} = \begin{bmatrix} K_{11} & K_{12} & 0 \\ K_{21} & K_{22} & 0 \\ 0 & 0 & K_{33} \end{bmatrix} \cdot \begin{bmatrix} \Delta X \\ \Theta \\ \Delta Y \end{bmatrix}$$

Where:

$$K_{11} = \sum \frac{1}{\Delta_i'}\left[\frac{4\lambda_i^{\,3}}{k_s d_i} + \frac{\ell_i}{E_i I_i}\right]$$

$$K_{12} = K_{21} = \sum \frac{1}{\Delta_i'}\left[\frac{2\lambda_i^{\,2}}{k_s d_i}\left(1 + 2\lambda_i \ell_i\right) + \frac{\ell_i^{\,2}}{2E_i I_i}\right]$$

$$K_{22} = \sum \frac{E_i A_i}{h_i} + \sum \frac{1}{\Delta_i'}\left[\frac{2\lambda_i}{k_s d_i}\left(1 + 2\lambda_i \ell_i + 2\lambda_i^{\,2}\ell_i^{\,2}\right) + \frac{\ell_i^{\,3}}{3E_i I_i}\right]$$

$$K_{33} = \sum \frac{E_i A_i}{h_i}$$

$$\Delta_i' = \frac{1}{3k_s d_i E_i I_i}\left(3 + 6\lambda_i \ell_i + 6\lambda_i^{\,2}\ell_i^{\,2} + 4\lambda_i^{\,3}\ell_i^{\,3} + \lambda_i^{\,4}\ell_i^{\,4}\right)$$

The equations can be written to solve for the displacements and rotation as follows:

$$\begin{bmatrix} \Delta X \\ \Theta \\ \Delta Y \end{bmatrix} = \begin{bmatrix} F_{11} & F_{12} & 0 \\ F_{21} & F_{22} & 0 \\ 0 & 0 & F_{33} \end{bmatrix} \cdot \begin{bmatrix} T \\ M \\ N \end{bmatrix}$$

Where:

$$F_{11} = F_{tx} = \frac{K_{11}}{\psi}$$

$$F_{22} = F_{rz} = \frac{K_{22}}{\psi}$$

$$F_{12} = F_{21} = F_{rz\_tx} = F_{tx\_rx} = \frac{-K_{12}}{\psi}$$

$$F_{33} = F_{ty} = \frac{1}{K_{33}}$$

$$\psi = K_{22}K_{11} - K_{12}^{\,2}$$

The above flexibility coefficients represent the flexibility of the substructure at the top of the shafts/columns and do not represent the effect of the cap thickness. The following formulas represent the adjusted flexibility of the substructure at the top of the cap:

$$F'_{11} = F'_{tx} = F_{11} + 2F_{12}t_{cap} + F_{22}t_{cap}^{\ 2}$$

$$F'_{22} = F'_{rz} = F_{22}$$

$$F'_{12} = F'_{21} = F'_{rz\_tx} = F'_{tx\_rz} = F_{12} + F_{22}t_{cap}$$

$$F'_{33} = F'_{ty} = F_{33}$$

Similar calculations are performed for the displacement in the longitudinal direction to obtain the associated rotation, translation and cross-term flexibility coefficients. The coefficients can then be placed in the 6x6 stiffness matrix based on the local axis of the member being defined. For the rotational flexibility about the vertical axis, an arbitrary value was applied to the flexibility matrix because it does not affect the results of the load distribution factors or the superstructure rotational stiffness values being investigated. Great care needs to be taken to ensure that the coefficients are placed in the correct location in the flexibility matrix. In addition, the correct sign needs to be provided for the off diagonal cross terms based upon the local axis of the member.

CONCLUSIONS AND RECOMMENDATIONS

The primary objective of the analysis was to determine the longitudinal rotational stiffness of the superstructure which prevents the longitudinal rotation of the top of the bent and reduces the P-delta affects thus reducing the design moment in the shafts and columns. The results of the bridge modeling indicate that longitudinal rotational stiffness of the superstructure is influenced by three elements – the bearings, the diaphragm and the adjacent pier continuity. However, the longitudinal rotation stiffness of the superstructure can be easily expressed as a percentage of the rotational stiffness provided by the two rows of bearing, which is essentially the summation of the axial stiffness of each bearing multiplied by the square of its distance from the centerline of the pier.

For the condition where the beams were continuous over the piers, the rotational stiffness of the superstructure is approximately 95% of the rotational stiffness of the bearings. For the interior piers with the typical diaphragms, simply supported beams and the continuous deck (Figure 8a), the superstructure stiffness was affected by the continuity of the adjacent piers. If both of the adjacent piers are interior piers, the superstructure stiffness is approximately 80% of the stiffness of the bearings. If one of the adjacent piers is an expansion pier and one is an interior pier, the superstructure stiffness is approximately 70% of the bearing stiffness.

If both of the adjacent piers are expansion joint piers, the superstructure stiffness is approximately 55% of bearing stiffness.

For the design of the expansion joint piers, the rotational superstructure stiffness was ignored. Although the bearings provide some rotational stiffness about their own axis, under ultimate conditions there is some concern about partial uplift of portions of the bearing due to rotations and deflections of the substructure and superstructure. However, under service conditions, the summation of the rotational stiffness of each bearing about its centerline can be used for the longitudinal rotational superstructure stiffness.

The secondary object of the analysis was to determine the distribution of the transverse and longitudinal loads to each pier. Standard practice is to isolate each unit and distribute the loads based on the relative stiffness of each pier. When doing this, the stiffness of the expansion joint piers are multiplied by 50% to account for the load being applied to these piers from the adjacent units. The results of the model generally confirm this process. The load distribution factors obtained from the GTSTRUDL model are generally within 5% of the factors obtained by the relative distribution method typically used.

Despite the 20% increase in the wind loading, by incorporating the rotational stiffness of the superstructure in the design of the bents, the reinforcement in the columns and shafts was actually reduced and, for some piers, the shaft and column diameter were also reduced. Estimates indicate that the reduction in the concrete and reinforcement reduced the construction cost approximately $1M from the proposal design.

The results of this analysis indicate that the incorporation of the superstructure's rotational stiffness can be easily applied to all bridge projects, resulting in significant cost savings without the need for any complex modeling. By simply calculating the rotational stiffness of the two rows of bearings and applying the appropriate reduction factors described above, the rotational stiffness of the superstructure can be included in the substructure design. This relatively simple procedure reduces the P-delta effects and the maximum bending moment in the substructure components, thus allowing for the optimization of the member sizes and reinforcing requirements. The attached design example illustrates the simple calculations required to calculate the superstructure stiffness and its effect on the substructure forces.

REFERENCES

1. Roeder, C. W., Stanton, J. F., and Taylor, A. W., "Performance of Elastomeric Bearings," *NCRP Report 298*, Oct. 1987.
2. Hetenyi, M., "Beams on Elastic Foundation" The University of Michigan Press, 1946.

JACOBS	Project	2007 PCI Convention	Sheet No.		Of
	Subject	Design Example - Rotational Stiffness of Superstructure	Authored By	JSH	Date Sep 2007
			Checked By		Date

Objective

Determine the longitudinal rotation stiffness of the superstructure and its affect on the substructure design.

Codes and Specifications

"AASHTO LRFD Bridge Design Specifications "American Association of State Highway and Transportation Officials (AASHTO), 1998 Edition, with interims thru 2003.

"Florida Department of Transportation Structures Design Guidelines for Load and Resistance Factor Design," 2004 Edition

"Florida Department of Transportation Standard Specifications for Road and Bridge Construction," 2004 Edition and Supplements thereto.

References

Roeder, C.W., Stanton, J.F., and Taylor, A.W. (1987). "Performance of Elastomeric Bearings." *National Cooperative Highway Research Program Report 298*, Transportation Research Board, Washington D.C.

Roeder, C.W., and Stanton, J.F. (1982). "Elastomeric Bearing Design, Construction, and Materials." *National Cooperative Highway Research Program Report 248*, Transportation Research Board, Washington D.C.

Unit & Function Definitions

Metric Units:

$kN \equiv 1000 \cdot newton \qquad MPa \equiv 1 \cdot 10^{6} \cdot Pa \qquad GPa \equiv 1 \cdot 10^{9} \cdot Pa$

English Units

$pcf \equiv \frac{lbf}{ft^3} \qquad psf \equiv \frac{lbf}{ft^2} \qquad plf \equiv \frac{lbf}{ft} \qquad kip \equiv 1000 \cdot lbf \qquad ksi \equiv \frac{kip}{in^2} \qquad klf \equiv \frac{kip}{ft} \qquad ksf \equiv \frac{kip}{ft^2} \qquad kcf \equiv \frac{kip}{ft^3}$

Functions

$maxval(a, b) \equiv if(a > b, a, b)$

$minval(a, b) \equiv if(a > b, b, a)$

Design Parameters

I. Background/Theory

- For two rows of bearings, subjected to a beding moment, the following equations of equilibrium and deformations can be defined:

$$M = (2 \cdot m + 2 \cdot p \cdot d) \cdot n$$

$$\theta = \frac{\Delta_c}{d}$$

Δ_c = vertical deflection of bearings

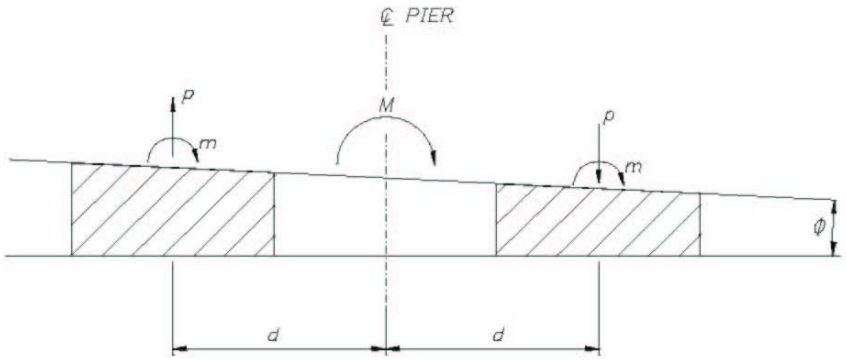

- Using the rotational and axial stiffness coefficients for neoprene bearings from Roederer and Stanton, the moment and axial load in the bearings can be written in terms of the stiffness and deformation as follows:

$$m = \frac{3 \cdot G \cdot \left(1 + 2 \cdot k \cdot S^2\right) \cdot I}{h_{rt}} \cdot \theta \qquad P = \frac{3 \cdot G \cdot \left(1 + 2 \cdot k \cdot S^2\right) \cdot A}{h_{rt}} \cdot \Delta_c$$

Where:
- G = shear modulus of elasticity of neoprene
- h_{rt} = total thickness of elastomer
- n = number of bearings per row
- A = plan area of bearing
- I = plan moment of inertia about axis of bending
- S = shape factor of bearing
- k = coefficient dependent on neoprene hardness

k = 0.75 for 50 durometer hardness
k = 0.60 for 60 durometer hardness
k = 0.55 for 70 durometer hardness

Substituting for *m* and *f* gives...

$$M = 2n \cdot \left[\frac{3 \cdot G \cdot \left(1 + 2 \cdot k \cdot S^2\right) \cdot I}{h_{rt}} \cdot \theta\right] + 2 \cdot n \cdot \left[\frac{3 \cdot G \cdot \left(1 + 2 \cdot k \cdot S^2\right) \cdot A}{h_{rt}} \cdot \Delta_c \cdot d\right]$$

Substituting for Δ_c in terms of θ gives...

$$M = 2n \cdot \left[\frac{3 \cdot G \cdot \left(1 + 2 \cdot k \cdot S^2\right) \cdot I}{h_{rt}} \cdot \theta\right] + 2 \cdot n \cdot \left[\frac{3 \cdot G \cdot \left(1 + 2 \cdot k \cdot S^2\right) \cdot A}{h_{rt}} \cdot \theta \cdot d^2\right]$$

I. Background/Theory

Simplifying the equation by combining terms...

$$M = 6 \cdot n \cdot \left[\frac{G \cdot \left(1 + 2 \cdot k \cdot S^2\right)}{h_{rt}} \right] \cdot \left(1 + A \cdot d^2\right) \cdot \theta$$

The above equation provides the rotational stiffness of the two rows of bearings

$$K_\theta = \frac{6 \cdot n \cdot G \cdot \left(1 + 2 \cdot k \cdot S^2\right) \cdot \left(1 + A \cdot d^2\right)}{h_{rt}}$$

II. Design Example - Superstructure Rotational Stiffness

- The following example is of a pier with six simply supported beams. The longitudinal spacing of the bearings is 1'-3" from the centerline of the pier.

A. Bearing Properties & Dimensions

Shear Modulus of Elasticity, G	$G := 14.4 \cdot ksf$	
Hardness Coefficient, k	$k := 0.75$	*(50 durometer hardness)*
Number of Bearings Per Row, n_{brg}	$n_{brg} := 6$	
Number of Rows, n_{row}	$n_{row} := 2$	
Transverse Dimension of Bearing, b_{brg}	$b_{brg} := 22 \cdot in$	
Longitudinal Dimension of Bearing, l_{brg}	$l_{brg} := 12 \cdot in$	
Plan Area of Bearing, A_{brg}	$A_{brg} := b_{brg} \cdot l_{brg}$	$A_{brg} = 264\,in^2$
Longitudinal Spacing of Rows, s_{rows}	$d_{brg} := 15 \cdot in$	
Thickness of Interior Neoprene Layer, t_{int}	$t_{int} := \frac{1}{2} \cdot in$	
Thickness of Exterior Neoprene Layer, t_{ext}	$t_{ext} := \frac{1}{4} \cdot in$	
Number of Interior Layers	$n_{int} := 6$	

II. Design Example - Superstructure Rotational Stiffness

B. Rotational Stiffness of Bearings

Shape Factor

$$S_{brg} := \frac{A_{brg}}{2 \cdot t_{int} \cdot \left(l_{brg} + b_{brg}\right)} \qquad S_{brg} = 7.765$$

Moment of Inertia

$$I_{long} := \frac{1}{12} \cdot b_{brg} \cdot l_{brg}^{3} \qquad I_{long} = 3168\,in^4$$

Neoprene Thickness

$$h_{rt} := n_{int} \cdot \left(t_{int}\right) + 2 \cdot \left(t_{ext}\right) \qquad h_{rt} = 3.5\,in$$

Rotational Stiffness

$$K_\theta := \frac{6 \cdot n_{brg} \cdot G \cdot \left(1 + 2 \cdot k \cdot S_{brg}^{2}\right) \cdot \left(I_{long} + A_{brg} \cdot d_{brg}^{2}\right)}{h_{rt}} \qquad K_\theta = 490369 \frac{kip \cdot ft}{rad}$$

C. Substructure Model

A FBPIER model was created for Pier 49 which has the dimensions shown in the attached sketch. The AASHTO loads were applied and the design moments were obtained in the columns/shafts for two models - one with the superstructure stiffness and one ignoring the stiffness. Pier 49 is an interior pier that has a backstation interior pier and an expansion joint pier for the ahead station pier. Therefore, the rotation stiffness of the superstructure is 70% of the value calculated above. A rotational spring was applied to each bearing which was equal to 70% of the above number divided by the number of bearings. The attached graph provides a comparison of the longitudinal bending moments in the columns/shafts. As the graph indicates, by including the superstructure stiffness, there is a 35% reduction in the longitudinal bending moment. Considering the transverse moments as well, this equates to a 30% reduction in the total bending moment in the columns/shafts.

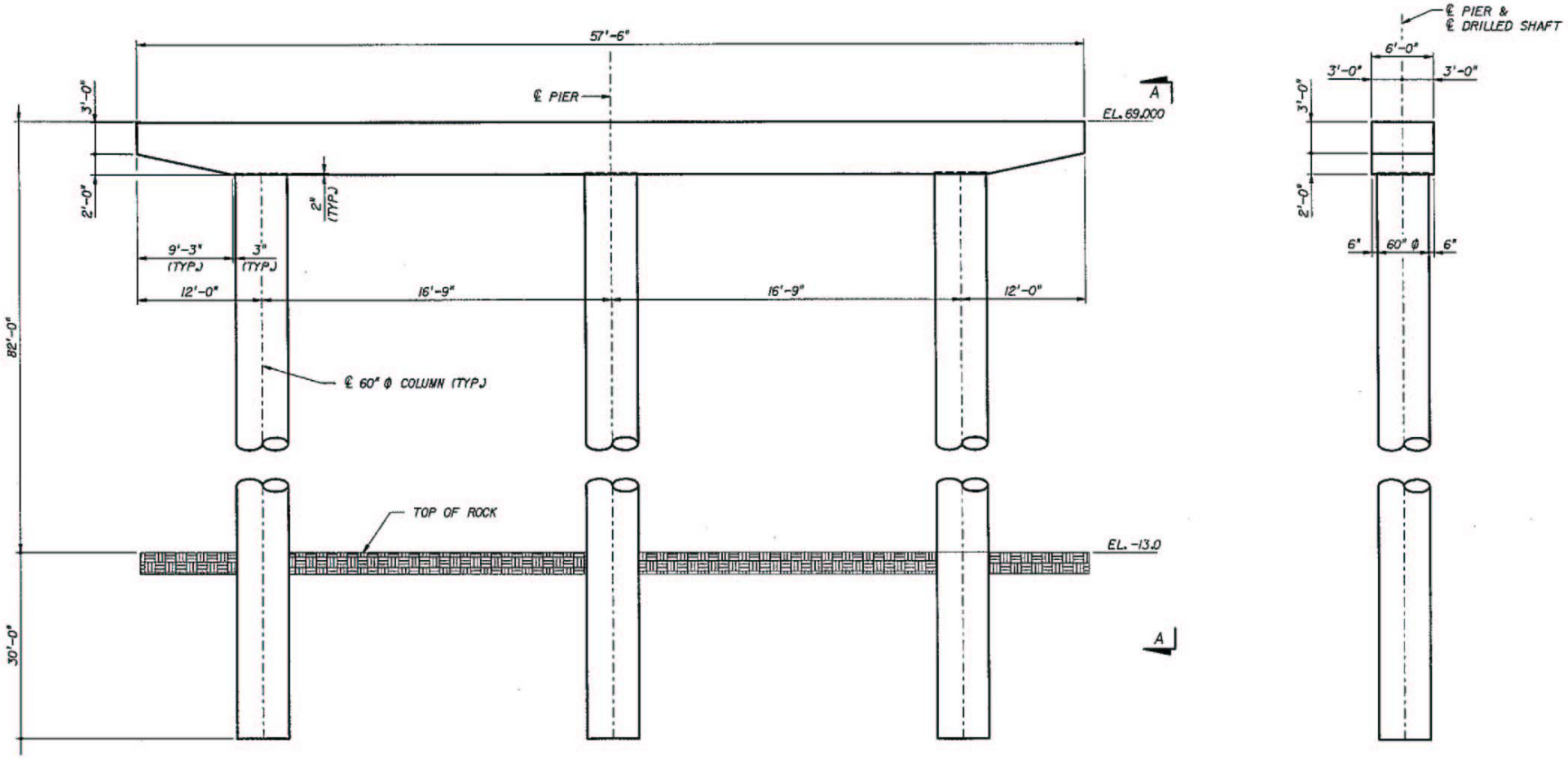

ELEVATION

VIEW A-A

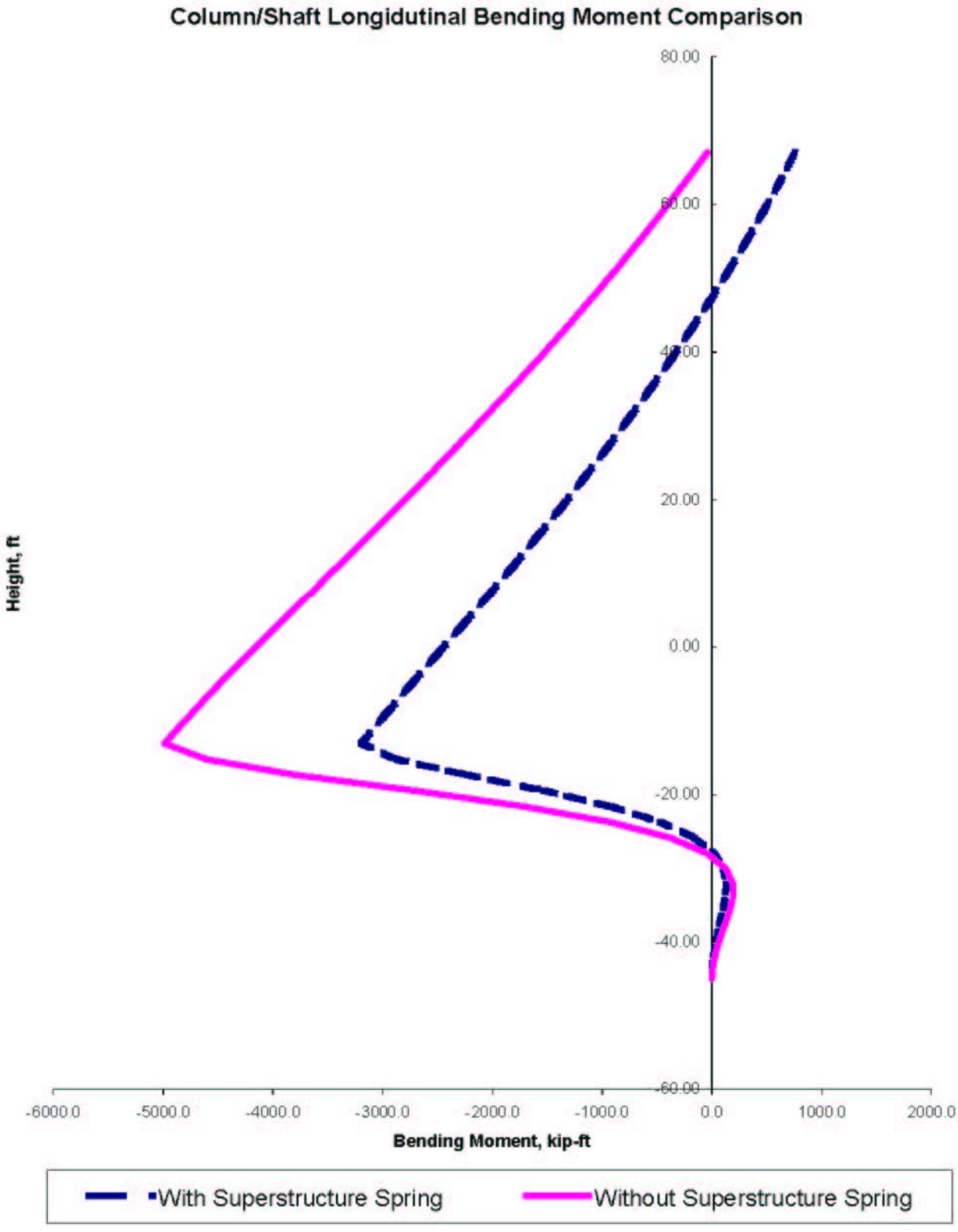
Column/Shaft Longidutinal Bending Moment Comparison
80.00
60.00
40.00
20.00
0.00
-20.00
-40.00
-60.00
Height, ft
-6000.0
-5000.0
-4000.0
-3000.0
-2000.0
-1000.0
0.0
1000.0
2000.0
Bending Moment, kip-ft
With Superstructure Spring
Without Superstructure Spring